Chemical Physics 46 (1980) 215–229

PROTON CONDUCTION IN LINEAR HYDROGEN-BONDED SYSTEMS

E.-W. KNAPP, K. SCHULTEN and Z. SCHULTEN
Max-Planck-Institut für biophysikalische Chemie, D 3400 Göttingen - Nikolausberg, FRG

Received 9 April 1979

It has been suggested that the hydrophilic side groups of proteins can form hydrogen-bonded conductors that transport protons across biomembranes. Based on previous studies of the proton dynamics in ice, a kinetic model for such proton conductors is developed. The steady-state proton current is evaluated as a function of the pH and voltage difference along the conductor. This electrochemical potential is found to determine the mechanism by which the protons are transported. Under acidic conditions the proton current is inversely proportional to the number of side groups composing the conductor and is determined by the rate of injecting a L-Bjerrum orientation fault into the hydrogen-bonded conductor. For small voltages (< 100 mV) an analytical expression for the proton flux is derived.

1. Introduction

In 1961 Mitchell [1] put forward the hypothesis that an active transport of protons across biomembranes is coupled to biological energy transduction in mitochondria and chloroplasts. Although experimental support of his hypothesis has been obtained, for example in the study of the light-driven proton pump of halobacterium halobium and in photosynthesis (for a review, see refs. [2] and [3], respectively), the molecular mechanism for the proton transport in these systems is still not fully understood.

Applying an analogy from proton motions in water and ice, Onsager suggested that protons could move through biomembranes utilizing the hydrophilic side groups of membrane proteins [4] as shown in fig. 1: the protein P spans the membrane and the hydrophilic side groups labeled X, Y, Z form a one-dimensional hydrogen bridge network to transport protons from side A to side B of the membrane. The group X–H, for example, may be the hydroxyl end of serine or the carboxyl end of glutamic acid. For halobacterium halobium this idea of proton conduction was given further support by the calculations of Dunker and Marvin [5,6] who determined that the pitch of two adjacent α-helices allows such a conducting pathway to exist. Recently Nagle and Morowitz [7–9] have suggested that this molecular concept may be the fundamental

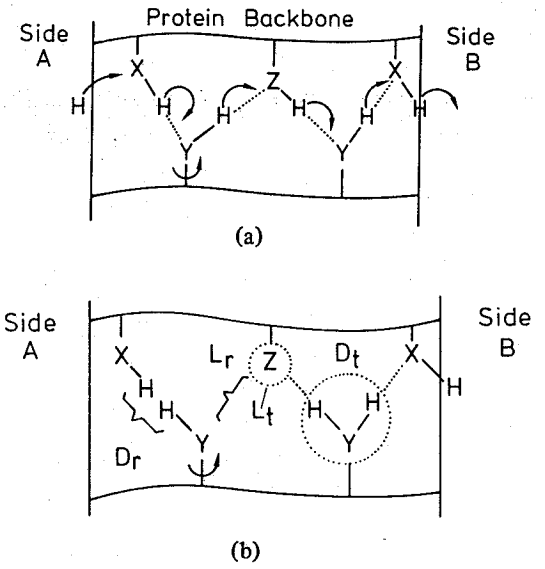

Fig. 1. (a) The side groups X, Y, Z of a protein spanning a biomembrane form a one-dimensional proton conductor. (b) Possible ionic (D_t, L_t) and orientation (D_r, L_r) defects in the hydrogen-bonded structure.

pathway for proton exchange in many biological systems and using a simplified statistical description of the proton dynamics, they determined the time it takes a proton to cross a membrane once it is injected into the network.

The motion of protons in such one-dimensional sys-

tems can be described in roughly two ways [10]: If the protein structure is rigid and the temperature sufficiently low, then tunneling or cooperative jumping between the groups establishes the proton conduction as had been calculated by Fischer et al. [11]. At physiological temperatures, proteins are probably more fluid like, and one can assume that transport occurs by a combination of thermally activated processes: jumping of protons between two groups or rotation of a group XH about the single bond P–X. Given the rates for these activated processes a statistical description can be given to the proton conduction. It is this latter statistical description which we will adopt in our paper. Similar models have been suggested previously to describe proton conduction in other one-dimensional hydrogen-bonded networks as in imidazole [12] and lithium hydrazinium sulfate crystals [13].

In this paper we evaluate the steady-state flux of protons through a one-dimensional passive conductor as a function of its length and electrochemical proton gradient across the membrane. Using the concepts developed to describe proton dynamics in ice, the kinetic model for the motion in the conductor is stated in section 2. The kinetic rates describing the transitions between the various states of protonation of the conductor are determined in section 3. The protonation and deprotonation rates for the conductor end groups as a function of the solution pH are derived in section 4. Modifications of the rates upon applying an electric field across the membrane are given in section 5. On the basis of the steady-state proton flux through the conductor, defined in section 7, we study in section 8 how chemical (pH) and electrical potential differences along the conductor affect the proton transport.

The aim of this paper is to provide a general kinetic framework for the description of proton conduction by amino acid side groups in proteins and to discuss the essential many-particle features of the conduction process, i.e. the cycles of proton configurations constituting the conduction pathway. Our treatment, contrary to previous approaches, is not restricted to certain ranges of the rate constants for the elementary transport processes. However, in lieu of a consistent set of rate constants for protein systems we chose to apply our theory to a hypothetical one-dimensional conductor governed by the rate constants of proton transport in ice. As this conduction is truely three-dimensional, our results convey only to a limited extent information on this system. Since our theory applies only to one-dimensional, thermally activated proton conduction, we do not like to pursue proton conduction in ice very far. Nevertheless, we have engaged in detailed discussions on how to abstract rate constants for the ice system to illustrate how corresponding rate constants may be obtained for protein side groups. In this respect studies on biological proton conduction certainly can gain much from the extended work on proton conduction in ice. In fact, most of our expressions employed for the rate constants governing proton transport between water molecules and ions can be applied also to amino acid side groups.

2. Description of the model

In the following we will consider the proton conductor crossing a membrane to be a linear arrangement of groups P–XH linked by hydrogen bridges and fixed at the protein backbone. As shown in fig. 1, we assume all of the groups to have two binding sites and therefore four different states of protonation. The states of protonation have their analogs in water or ice. For example, $P–X^-$ corresponds to OH^-, $P–XH_2^+$ to H_3O^+, and the two states P–XH to H_2O. The states XH_2^+ and X^- are considered to be ionic faults, and since the faults can move only by *translation* of a proton to another group, they are labeled D_t and L_t faults, respectively (see for example, ref. [14]). Between the conductor elements, Bjerrum type faults can exist. For example, the absence of protons between the groups Y and Z gives rise to a Bjerrum L-fault and the presence of two protons between the groups X and Y establishes a Bjerrum D-fault. These faults move by *rotation* of the group YH about the P–Y bond and, hence, are labeled D_r and L_r [14,15].

For a conductor with N groups, each with two binding sites, there are 2^{2N} possible ways (proton configurations) of distributing up to $2N$ protons within the one-dimensional conductor. The dynamics of the proton motion in a linear conductor of several elements can be described by the master equation

$$\mathrm{d}\boldsymbol{P}/\mathrm{d}t = \boldsymbol{P}\mathbf{K}\,, \tag{2.1}$$

where $\boldsymbol{P}$ is a row vector of maximum dimension 2^{2N}. The component P_j is to represent the probability that the jth proton configuration occurs, e.g. the probabil-

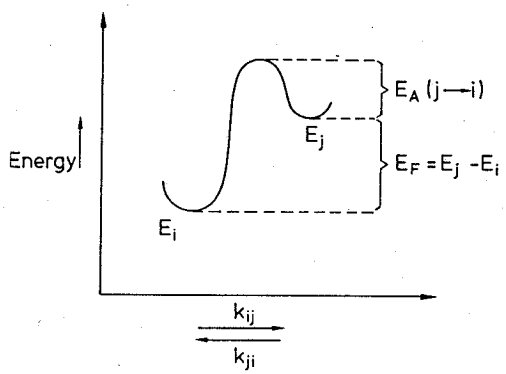

Fig. 2. Activation energy diagram for the first-order transition rate constants K_{ij}: $E_A(i \to j) = E_A(j \to i) + E_F$.

ity that no proton is found in the conductor. The elements of the matrix **K** are the first-order rate constants describing the occurrence of transitions between the proton configurations of the conductor. For transitions involving a jump or reorientation of a proton within the chain, the rate constants are written in the Arrhenius form

$$K_{ij} = A_{ij} \exp[-\beta E_A(i \to j)], \tag{2.2}$$

where $\beta = 1/kT$, and $E_A(i \to j)$ and A_{ij} are the activation energy and the pre-exponential factor for the transition $i \to j$, respectively (see fig. 2). Throughout the article, a temperature T of 298 K will be assumed. The conservation of total probability, $\Sigma_j \, dP_j/dt = 0$, requires that the elements of the rate matrix satisfy the relation

$$K_{ii} = -\sum_{j \neq i} K_{ij}. \tag{2.3}$$

Condition (2.3) guarantees the existence of a non-trivial steady-state solution of the master equation (2.1).

In order to calculate the first-order rate constants K_{ij}, we will make the following restrictive assumptions: (i) *the defects in the conductor do not interact with each other,* (ii) *the different states of a conductor are connected by elementary transitions which involve only the rotation of a single group or translation of a single proton between two adjacent groups.* The first restriction implies that the energy of a configuration or state is equal to the sum of energies for each defect appearing in the configuration and that the faults move independently as long as they do not recombine. The two states having no faults will be assigned a zero energy of formation. With the second assumption we are neglecting concerted motions of the protons whereby a fault migrates over more than one element in a single transition. We do not, for example, consider the tunneling of an ionic D_t fault. In fact, Chen et al. [16] have indicated that proton tunneling does not play an important role for ionic-transport in ice for not too low temperatures.

The number of possible proton configurations for a conductor with N components is 2^{2N}. For a short conductor of three elements (length ≈10 Å), the transition rates K_{ij} between the 64 states can be analyzed in a straightforward, but tedious manner. Since membranes more realistically are 20–50 Å wide, we developed a computer algorithm that automatically determines the proton configurations and the elements K_{ij} of the rate matrix.

The proton configurations (labeled by integers l) are best represented by the binary number

$$N_c(l) = a_1^{(l)} a_2^{(l)} \ldots a_{2N}^{(l)}, \tag{2.4}$$

where the digit $a_m^{(l)}$ gives the number of protons, 0 or 1, at the mth binding site in the lth configuration. For example, for $N = 2$ the configuration with all four protons is represented by $N_c = 1111$. The transformation of one conductor state to another by rotation, translation, uptake or release of a single proton corresponds to changes of the integer N_c.

3. Evaluation of the first-order transition rates

With the foregoing simplifications, the change in the state of the conductor resulting from the motion of a single proton can be described by one of 10 elementary transitions: four correspond to migrations of a single D or L fault; four to the creation of the single faults L_r or D_r and the fault pairs L_tD_t and L_rD_r; and two to the creation of a D_t or L_t fault by protonation or deprotonation of the conductor end groups. The migrations are denoted by D → D or L → L and the fault creations by $0 \to L_t$, $0 \to D_t$, $0 \to L_r$ or $0 \to D_r$ where 0 refers to the initial state of the conductor (before the new fault was created). For example, the rotation of the YH group in fig. 1 results in the disappearance of a D_r fault, i.e. is written $L_rD_r \to 0$.

Every element K_{ij} of the rate matrix will describe one of these 10 transitions. To evaluate K_{ij}, the activation energies for each type of transition must be

Table 1
Energy of formation and activation of pair defects in ice at 263 K (in eV)

	Bjerrum (L_rD_r) defect	Ionic (L_tD_t) defect
energy of formation	0.68 [17] 0.72 [21]	0.96 [17] 1.0 [21]
activation energy of diffusion	0.235 [17] 0.24 [21]	≈0.02 [20] 0.05, 0.10 [18] a) 0.10 [19] b)

a) Activation energies for L_t and D_t migration measured in doped ice.
b) Activation energy of recombination of L_t and D_t faults (neutralization) in water at $T = 298$ K.

known. Unfortunately, the activation energy for fault migration and the energies of fault formation have been well studied only for ice and even in this case due to experimental difficulties there is little consensus as to the values of these quantities. We use the available information for ice as our reference data, and derive the necessary modifications to treat conductors composed of heterogeneous hydrophilic groups.

Table 1 contains the information on the formation and motion of the faults L_tD_t and L_rD_r in ice. The activation energy E_A of diffusion corresponds to the migration of the more mobile D or L fault. On the basis of the observed ratio of the mobilities $\mu(L_r)/\mu(D_r) \approx 1.5$ (ref. [17]), we assign in table 2 the same activation energies of migration (E_M) to the Bjerrum L and D faults.

Since the activation energies of migration of the ionic faults, $D_t = H_3O^+$ and $L_t = OH^-$, are extremely small, the ratio of the mobilities could only be determined to fall in the range $1 < \mu(H_3O^+)/\mu(OH^-) < 10$ (refs. [17,18,22]). Jaccard [20] has estimated that $E_M(D_t)$ is about 0.02 eV, and we arbitrarily set $E_M(L_t)$ at 0.04 eV.

If we liken the formation of an ionic fault pair L_tD_t to the autodissociation reaction of water [14],

$$2\,H_2O \rightleftharpoons H_3O^+ + OH^-, \tag{3.1}$$

we can define an energy of formation based on its equilibrium constant

$$K_{eq} = \exp[-\beta E_F(L_tD_t)] = [H_3O^+]\,[OH^-]/[H_2O]^2, \tag{3.2}$$

where we have taken the concentration of $[H_2O] \approx 55.5$ mol ℓ^{-1} and $[H_3O^+]\,[OH^-] = 10^{-14}$. It is convenient for the later modifications in treating conductors with heterogeneous hydrophilic groups to express the autodissociation reaction in terms of the competing elementary dissociation processes

$$H_3O^+ \rightleftharpoons H_2O + H^+, \quad pK(H_3O^+), \tag{3.3}$$

$$H_2O \rightleftharpoons OH^- + H^+, \quad pK(H_2O). \tag{3.4}$$

The equilibrium constant K_{ion} for the first reaction defines $pK(H_3O^+) = -\log K_{ion} = -1.745$, the second reaction defines $pK(H_2O) = 15.745$. Here and throughout the paper the pK value of a conductor group XH, pK(XH), will be understood to refer to the equilibrium of the reaction

Table 2
Energy of formation and activation of elementary motions of defects assumed for our one-dimensional proton conductor (in eV)

Energy	D_t	L_t	D_r	L_r	D_tL_t	D_rL_r
energy of formation E_F	0.52 a) (0.24) b)	0.52 a) (0.18) b)	0.5	0.2	1.03 (0.41) c)	0.7
activation energy of migration E_M	0.02	0.04	0.24	0.24	–	–
activation energy of destruction E_D	0.02	0.04	0.24	0.24	0.02	0.24

a) Energy of formation based on water using eqs. (4.16) and (4.17) with pK(XH) = 15.745, $pK(XH_2^+) = -1.745$ and pH = 7.
b) Energy of formation using eqs. (4.16) and (4.17) with pK(XH) = 10, $pK(XH_2^+) = 3$ and pH = 7.
c) Energy of formation using eq. (3.11) with pK(XH) = 10 and $pK(XH_2^+) = 3$.

$$XH \rightleftharpoons X^- + H^+, \tag{3.5}$$

where

$$pK(XH) = -\log[X^-]\,[H^+]/[XH].$$

In doing so, we are suppressing the fact that our definition of pK is based on reactions in water. The energy of formation of the fault pair D_tL_t can now be expressed as a pK difference

$$E_F(L_tD_t) = 2.3\,[pK(H_2O) - pK(H_3O^+)]\,/\beta = 1.03\ \text{eV}. \tag{3.6}$$

The energy of formation of the single faults D_t and L_t which appear upon protonation and deprotonation of the conductor end groups will be defined in the following section.

Although the energy of formation of a Bjerrum fault pair L_rD_r is known, we do not know how to split it into contributions arising from the single faults. The proximity of the two protons between the adjacent groups in the orientation fault D_r (see fig. 1) should make it considerably less stable than a L_r fault. Various approximations have been made, and in setting $E_F(D_r) = 0.5$ eV and $E_F(L_r) = 0.2$ eV we are probably overestimating the latter [14,17].

To obtain activation energies of destruction for the two fault pairs L_tD_t and L_rD_r, and the two single faults L_r and D_r, we assume that their disappearance is just another example of an L or D migration. In the case of the fault pair, it is controlled by the mobility of the faster single fault migration

$$\begin{aligned} E_D(L_tD_t) &= E_M(D_t), \\ E_D(L_rD_r) &= E_M(D_r) = E_M(L_r), \\ E_D(L_r) &= E_D(D_r) = E_M(L_r), \end{aligned} \tag{3.7}$$

where E_D (E_M) denotes the activation energy for the disappearance (migration) of a fault. The activation energy of a fault creation is assumed to be the sum of E_F and E_D

$$\begin{aligned} E_A(0 \rightarrow \mathrm{LD}) &= E_F(\mathrm{LD}) + E_D(\mathrm{LD}), \\ E_A(0 \rightarrow \mathrm{L}) &= E_F(\mathrm{L}) + E_D(\mathrm{L}). \end{aligned} \tag{3.8}$$

The pre-exponential factor A_{ij} appearing in eq. (2.2) is taken to be the same for all the transitions in table 2. The rate of dissociation of H_2O has been determined in ice to be 3.2×10^{-9} s^{-1} at 263 K (ref. [17]). By virtue of the activation energy for the formation of an ionic fault pair given in table 2 and of eq. (2.2), we obtain $A = 5.1 \times 10^{10}$ s^{-1}. For simplicity we have adopted the value

$$A_{ij} = 10^{11}\ \text{s}^{-1} \tag{3.9}$$

throughout the paper. With this value of the pre-exponential factor, the rate constants for migration of an ionic D_t fault and a Bjerrum L_r fault are 5×10^{10} s^{-1} and 7×10^6 s^{-1}, respectively.

The assumption of identical frequency factors A_{ij} for L_r Bjerrum fault and D_t ionic defect transport is rather arbitrary and neglects the difference in entropic contributions between these processes. It appears that in ice these contributions counteract the difference in activation energies and bring about rate constants which are close in value. The effect of such behavior will be discussed briefly in section 8. For proton conduction in proteins one may expect that sterical effects slow down the rotation processes. On the other hand, proton translation between the amino acid side groups in proteins may also be governed by sterical effects (alignment of the groups) such that the rate constants for L_t defect migration may be slowed down to become close in value to the rate constants for L_r fault migration.

When the conductor is composed of heterogeneous hydrophilic groups, we assume that only the activation energies for ionic faults in table 2 must be modified. The transitions involving movement of an orientation fault L_r or D_r are supposed to be uneffected by the heterogeneity. The energy of formation for an ion fault pair $D_t^Y L_t^X$ can be estimated from the proton transfer reaction

$$XH + YH \rightleftharpoons X^- + YH_2^+. \tag{3.10}$$

Following the same procedure used above to determine $E_F(L_tD_t)$ for water [(cf. eqs. (3.1) to (3.6)], we can again express E_F by a pK difference

$$E_F(L_t^X D_t^Y) = 2.3\ [pK(XH) - pK(YH_2^+)]\,/\beta. \tag{3.11}$$

For the calculations presented in section 8, we have considered the conductor components to be homogeneous with values typical for protein side groups [23]

$$\begin{aligned} &pK(XH_2^+) = 3 \text{ rather than } pK(H_3O^+) = -1.745, \\ &pK(XH) = 10 \text{ rather than } pK(H_2O) = 15.745. \end{aligned} \tag{3.12}$$

Employing these values in eq. (3.11), one obtains $E_F(L_t^X D_t^Y) = 0.41$ eV indicated in parentheses in table 2.

Modifications of the activation energies of migration $D_t^X \rightarrow D_t^Y$ can be estimated by considering the proton transfer reaction

$$XH_2^+ + YH \rightleftharpoons XH + YH_2^+, \tag{3.13}$$

where $K_{eq} = 10^{-[pK(XH_2^+) - pK(YH_2^+)]}$. When the groups X and Y are not the same, or rather when $pK(XH_2^+) \neq pK(YH_2^+)$, the migration potentials are no longer symmetric. We allow for this asymmetry by modifying only one of the activation barriers. If $pK(XH_2^+) > pK(YH_2^+)$ then

$$E_A(YH_2^+ \rightarrow XH_2^+) = E_A(D_t^Y \rightarrow D_t^X) = 0.02 \text{ eV},$$

$$E_A(XH_2^+ \rightarrow YH_2^+) = E_A(D_t^Y \rightarrow D_t^X) + 2.3\,[pK(XH_2^+) - pK(YH_2^+)]/\beta. \tag{3.14}$$

Similar logic is used to make corrections for the L_t fault migrations. If $pK(XH) < pK(YH)$

$$E_A(Y^- \rightarrow X^-) = E_A(L_t^Y \rightarrow L_t^X) = 0.04 \text{ eV},$$

$$E_A(X^- \rightarrow Y^-) = E_A(L_t^Y \rightarrow L_t^X) + 2.3\,[pK(YH) - pK(XH)]/\beta. \tag{3.15}$$

4. Protonation and deprotonation rates

The end groups B of the proton conductor interact with an aqueous solution. In this section we will consider the injection and ejection of protons at the end groups, e.g. the creation of D_t and L_t faults described for example by the reactions

$$HX\,HB + H_3O^+ \rightleftharpoons HX\,HBH^+ + H_2O$$

and

$$XH\,BH + OH^- \rightleftharpoons XH\,B^- + H_2O.$$

Because of their bimolecular character these processes are governed by the concentration and diffusion of H_3O^+, H_2O and OH^- species and should also depend to some extent on electrostatic interactions at the membraneous surface around the end groups. We will assume that a proton from the solution cannot be introduced into an interstitial site and, consequently, that the protonation and deprotonation of the end group B can lead only to the formation or removal of an ionic defect. In principle, also the formation of L_r faults, e.g.

$$HX\,HB \rightleftharpoons HX\,BH$$

should be affected by the interaction with the aqueous solution. For the sake of simplicity, we will assume, however, that these processes, which are mainly of monomolecular character, can be described by the same rate constants as intrastitial L_r fault migration.

The rate constants for the uptake and release of protons by the conductor will depend on the pH values of the solution and the pK's of the conductor end components. The end group B, for example, can be protonated by the species H_3O^+ and H_2O and deprotonated by the species OH^- and H_2O according to the pair of parallel reactions:

$$B + H_3O^+ \underset{K_{-1}}{\overset{K_1}{\rightleftharpoons}} BH^+ + H_2O, \tag{4.1a}$$

$$B + H_2O \underset{K_{-2}}{\overset{K_2}{\rightleftharpoons}} BH^+ + OH^-, \tag{4.1b}$$

where B represents either the state $P{-}X^-$ or $P{-}XH$. The first-order rate constants of protonation K_P and deprotonation K_D describing the overall reaction

$$B \underset{K_D}{\overset{K_P}{\rightleftharpoons}} BH^+ \tag{4.2}$$

are

$$K_P = K_1[H_3O^+] + K_2[H_2O],$$
$$K_D = K_{-1}[H_2O] + K_{-2}[OH^-]. \tag{4.3}$$

To obtain the second-order rate constants $K_{\pm 1}$ and $K_{\pm 2}$, we have to consider reactions (4.1) in greater detail. Both reactions can be represented by the general reaction scheme

$$B + HA \underset{k_{1s}}{\overset{k_{1d}}{\rightleftharpoons}} \underset{C_1}{[B \ldots HA]} \underset{k_{21}}{\overset{k_{12}}{\rightleftharpoons}} \underset{C_2}{[BH \ldots A]} \underset{k_{2d}}{\overset{k_{2s}}{\rightleftharpoons}} BH^+ + A^-, \tag{4.4}$$

which includes the reactant and product intermediate

states, C_1 and C_2. HA denotes either the proton donor H_3O^+ or H_2O. The bimolecular forward rate constant k_f (K_1 or K_2) and the backward rate constant k_b (K_{-1} or K_{-2}) can now be expressed approximately as

$$k_f = k_{1d}\phi_{12}, \tag{4.5}$$

$$k_b = k_{2d}\phi_{21}, \tag{4.6}$$

where k_{id} is the bimolecular diffusion controlled reaction rate constant. (Our treatment holds as long as k_{1d} and k_{2d} are small compared to the other rate constants.) For neutral species k_{id} is [24]

$$k_{id} = 4\pi D_i r_i. \tag{4.7}$$

D_i is the relative diffusion coefficient and r_i the distance between the centers of the reacting species in the encounter complex. ϕ_{12} (ϕ_{21}) is the probability that the encounter complex $C_1(C_2)$ goes to the encounter complex $C_2(C_1)$ and breaks apart to give the products on the right (left).

If we treat the products and reactants as neutral species with the same relative diffusion constant D, so that $k_{1s} = k_{2s} = k_s$, then ϕ_{12} and ϕ_{21} have the simple forms

$$\phi_{12} = [1 + (k_{21} + k_s)/k_{12}]^{-1}, \qquad \phi_{21} = [1 + (k_{12} + k_s)/k_{21}]^{-1}. \tag{4.8}$$

Furthermore, in this case the rates k_{12} and k_{21} have a simple relationship to the equilibrium constant K_{eq}

$$K_{eq} = k_f/k_b = \phi_{12}/\phi_{21} = k_{12}/k_{21}. \tag{4.9}$$

Expressing the K_{eq} for reaction (4.4) by pK differences we can write

$$k_{12}/k_{21} = 10^{[pK(BH^+) - pK(HA)]}. \tag{4.10}$$

In applying the above treatment to eq. (4.1a) [eq. (4.1b)] the expression pK(AH) should be equated with pK(H_3O^+) [pK(H_2O)]. In applying eq. (4.10) to biological systems, it must be realized that pK values can be altered considerably by local protein and membrane environments. (This remark applies, of course, to all pK values entering the formulas in this paper.) The maximum of k_{12} and k_{21} will be the rate constant for the migration of a D_t fault between the solvent and the chain end. The value for $E_M(D_t)$ in table 2, and the pre-exponential factor given in section 3 ($A = 10^{11}$ s^{-1}) yield

$$\max(k_{12}, k_{21}) \doteq 5 \times 10^{10}\ \text{s}^{-1}. \tag{4.11}$$

We take this value also as a measure for the rate of separation of the encounter complex, i.e.

$$k_s = \max(k_{12}, k_{21}). \tag{4.12}$$

For values typical of proton exchange reactions, e.g. $D = 5 \times 10^{-5}$ cm^{-2} s^{-1} and $r = 10$ Å,

$$k_d = 4 \times 10^{10}\ \text{mol}^{-1}\ \text{s}^{-1}. \tag{4.13}$$

Assuming $k_s \gg \min(k_{ij}, k_{ji})$ in eq. (4.8), a condition fulfilled for the pK values adopted [i.e. eq. (3.12)], we can derive the following expressions for the protonation and deprotonation rates in (4.3)

$$K_P = 2[10^{10-pH} + 10^{pK(BH^+)-4}] \tag{4.14}$$

$$K_D = 2[10^{10-pK(BH^+)} + 10^{pH-4}]. \tag{4.15}$$

As long as $pH < 14 - pK(BH^+)$, the rates of proton uptake and release are primarily determined by the reaction in (4.1a). When $pH = pK(BH^+)$, K_P and K_D become identical. More general expressions which take into account the electrostatic interactions of the reacting species can be derived easily, but the simple formulas above contain the salient pH and pK dependences. For lack of information concerning the solvent–chain electrostatic interactions, all protonation and deprotonation processes have been evaluated according to eqs. (4.14) and (4.15), respectively, i.e. assuming free diffusion of the reactants. In particular, this simple treatment also neglects the increase in electrostatic energy required to take a proton from bulk water to the interior of a membrane protein with low dielectric constant. The concomitant reduction of the protonation rate may be counteracted (not under steady-state conditions) by a negative surface potential which attracts protons and, thereby, increases the effective proton concentration at the surface. The protonation and deprotonation of the conductor end group B = XH gives rise to the single ionic faults $D_t(XH_2^+)$ and $L_t(X^-)$. We use reaction (4.2) and the rates K_P and K_D to define energies of formation for these faults. For the reactions $XH + H_3O^+ \rightleftharpoons XH_2^+ + H_2O$ and $XH + H_2O \rightleftharpoons XH_2^+ + OH^-$ we obtain at pH = 7

$$K_P/K_D = 10^{pK(XH_2^+)-7} = \exp[-\beta E_F(D_t)], \tag{4.16}$$

and for the reactions $X^- + H_3O^+ \rightleftharpoons XH + H_2O$ and $X^- + H_2O \rightleftharpoons XH + OH^-$

$$K_D/K_P = 10^{7-pK(XH)} = \exp[-\beta E_F(L_t)]. \quad (4.17)$$

The energies of L_t and D_t formation appearing in table 2 are derived from these expressions.

5. Influence of an electric field

The transition rates and, consequently, the steady-state proton flux can be changed by applying an electric field across the membrane. The field will accelerate translations and rotations that move a proton in the direction of the field and slow down those that move it against the field. Assuming a homogeneous field inside the membrane, the potential at a distance x from the membrane surface will be

$$U(x) = U_A + x(U_B - U_A)/d, \quad (5.1)$$

where d is the width of the membrane, and U_A and U_B are the electric potentials at the surfaces A and B, respectively.

To move a charge q from x_1 to x_2 requires the energy $\Delta\mu(U_B - U_A)/d$, where $\Delta\mu = q(x_2 - x_1)$ is the change of dipole moment connected with the charge movement. It is important to realize that the charge of a conducted proton is not confined to the actual position of the proton, but rather is shared between the proton and the protonated site, i.e. the oxygen in case of ice and the amino acid side groups in case of proteins. For this reason the motion of the proton from x_1 to x_2 either by rotation or by translation is not accompanied by $\Delta\mu = e(x_2 - x_1)$, but by rather different changes of dipole moment μ_r and μ_t, respectively. Although $|x_2 - x_1|$ is larger for a rotation than for a translation one has $\mu_r/\mu_t = 0.56$ [25] ‡.

The conduction of a proton across the entire membrane corresponds to $\Delta\mu = ed$. For a conduction with N groups we consider this dipole moment to be partitioned

$$ed = N\mu_r + (N-1)\mu_t. \quad (5.2)$$

Assuming the minima of the transition potentials are symmetrically located about the potential maximum, the free energy of activation for rotations and translations moving H^+ against (with) the field $\overleftarrow{E}_A^{elect}$ ($\overrightarrow{E}_A^{elect}$) will exhibit an increase (decrease)

$$\overleftarrow{E}_A^{elect} = E_A + \mu|U_A - U_B|/2d,$$
$$\overrightarrow{E}_A^{elect} = E_A - \mu|U_A - U_B|/2d. \quad (5.3)$$

Here μ represents the change of dipole moment accompanying the respective transitions. By virtue of (5.2) one finds for a translation

$$\mu_t = ed\,[N(1 + \mu_r/\mu_t) - 1]^{-1} \quad (5.4)$$

and for a rotation

$$\mu_r = \mu_r(\mu_r/\mu_t), \quad (5.5)$$

i.e. only a knowledge of the ratio μ_r/μ_t is being required. The rates K_{ij} will be altered correspondingly

$$\overleftarrow{K}_{ij}^{elect} = K_{ij}\exp[-\beta\mu|U_A - U_B|/2d],$$
$$\overrightarrow{K}_{ji}^{elect} = K_{ji}\exp[\beta\mu|U_A - U_B|/2d]. \quad (5.6)$$

We assume that the electric field has no effect on the protonation and deprotonation reactions in eqs. (4.14) and (4.15), i.e. the potential of the solution A is the same as the potential of the membrane surface A. Furthermore, only electric field strengths that give rise to field corrections $\beta\mu|U_A - U_B|/2d$ smaller than the smallest activation energy $E_A = 0.02$ eV will be considered.

6. Selection of proton configurations

In order to keep for the sake of numerical effort the number of proton configurations small, three selection criteria have been employed against those configurations which do not contribute significantly to the proton conduction. Configurations are neglected

(1) if they entail more than either one L_r, D_t, L_t or L_rL_t fault;
(2) if the number of protons they contain deviates from the number of groups N of the conductor by more than one;
(3) if their energy of formation is larger than $E_F^{max} = 0.38$ eV.

The criteria are redundant in that, for example, $E_F = 0.38$ eV corresponds to the energy of formation of an L_rL_t fault (see table 2). The E_F^{max} value may be used to eliminate configurations allowed by the first

‡ This value of μ_r/μ_t corresponds to the ratio e_B/e_F in ref. [25] and strictly applies only to the three-dimensional ice structure.

two criteria. With these restrictions, the dimension of the rate matrix **K** can usually be reduced from 2^{2N} to $(N+1)^2$. In section 8 we will show under which pH conditions calculations employing the above restrictions reproduce those calculations accounting for all configurations.

7. Steady-state flux

The steady-state condition $dP/dt = 0$ reduces the master equation (2.1) to a homogeneous system of algebraic equations

$$P^0 \mathbf{K} = 0. \tag{7.1}$$

The flux of protons into the B end of the conductor $J_{B\to A}$ can be determined from the steady-state solution P^0 by means of

$$J_{B\to A} = K^B \cdot P^0, \tag{7.2}$$

where K^B is the vector with components

$$K_i^B = \pm K_{ij} \text{ if there exists a } j \text{ such that } N_c(i) - N_c(j) = \pm 1, \tag{7.3}$$

$$= 0 \quad \text{otherwise.}$$

In writing eq. (7.3) we have taken advantage of eq. (2.4) which assigns the protonation states on the right hand binding side in contact with solution B the binary digit a_{2N}, i.e. removal of a proton from B lowers the configuration label N_c by 1, adding a proton to B increases N_c by 1. Under steady-state conditions the flux at the A end of the conductor evaluated correspondingly must equal $J_{B\to A}$. This equality was used as a non-trivial test of our computations.

8. Results and discussion

The steady state proton flux $J_{B\to A}$ as defined in eq. (7.2) has been calculated for a one-dimensional conductor with a maximum of seven equal components assuming various external pH values and electric potentials. The transition rate constants K_{ij} as given by eqs. (2.2) and (5.6) were evaluated using the activation energies of table 2 for conductor groups with $pK(XH_2^+) = 3$ and $pK(XH) = 10$, and $A_{ij} = 10^{11}\ s^{-1}$. As discussed in section 3, the assumption of identical frequency factors

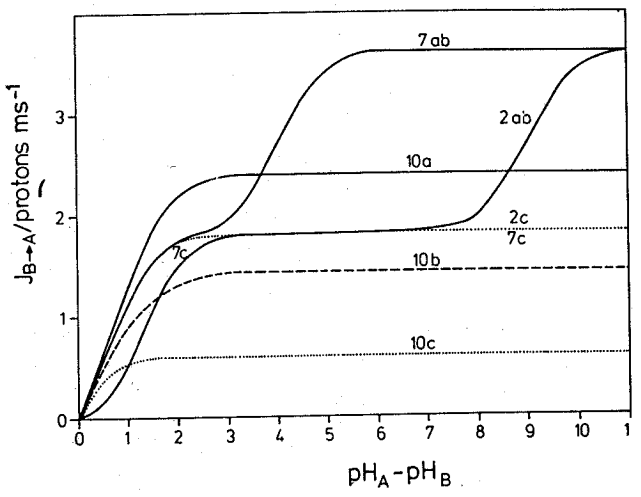

Fig. 3. Steady-state proton flux J_{BA} through a conductor of two groups as a function of $pH_A - pH_B$ at $pH_B = 2, 7, 10$. The proton configurations included in the calculations are those of the graphs in figs. 4a and 4b (——), in fig. 4b except the configuration 0000 (– – –), and in fig. 4c (...).

for rotation and translation processes gives rise to rate constants which differ by four orders of magnitude for these two processes. At the end of this section, we will discuss the situation when frequency factors are such that these rate constants are comparable in magnitude.

Figs. 3 to 5 represent for a conductor with 2 groups ($N = 2$) the evaluated proton flux from solution B to solution A as a function of the pH of the solutions on either side of the membrane (see fig. 1). In fig. 3 the flux resulting from calculations accounting for all 16 possible proton configurations (curve a) is compared to the flux predicted by calculations with the number of proton configurations reduced by a fault or energy criterion (curves b and c). The transitions connecting all 16 configurations are shown in fig. 4a. The energy criteria with $E_F^{max} = 0.38$ eV (only either one D_t, L_t, L_r, or L_tL_r fault allowed) and with $E_F^{max} = 0.24$ eV (only either one D_t, L_t, or L_r fault allowed) result in 9 and 7 proton configurations, respectively, as indicated in figs. 4b and 4c. Fig. 3 demonstrates that the flux resulting from the reduced configuration graph of fig. 4b (with the 0000 configuration excluded, however) approaches the flux as predicted by the complete calculation only as long as $pH_B < 7$. Agreement with the latter flux for a calculation based on the configurations in fig. 4c is found only for $pH_B < 7$ and $pH_A < 9$. The energetically more unfavourable configuration 0000

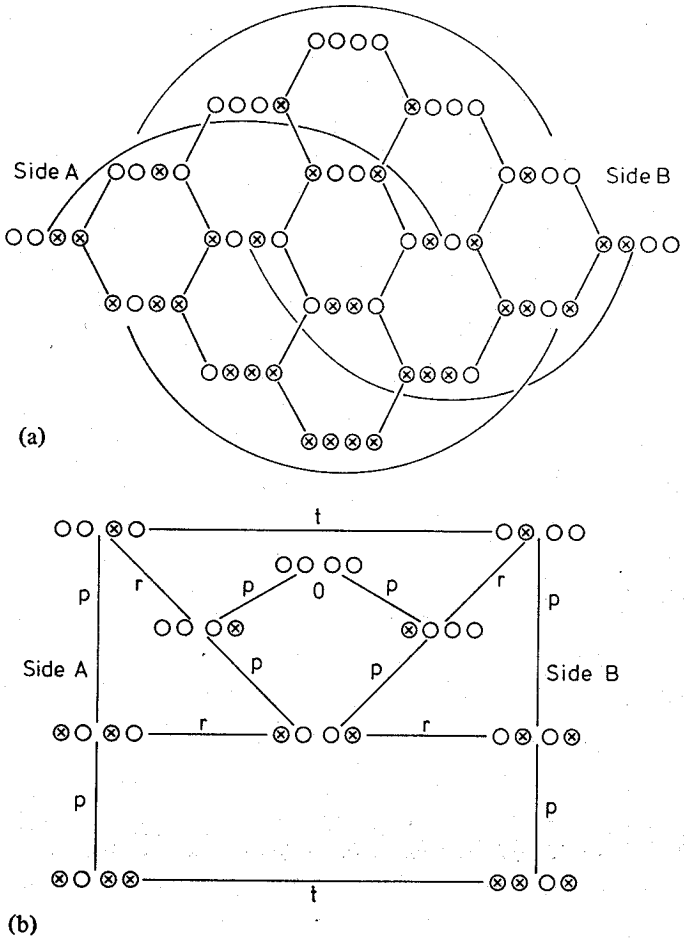

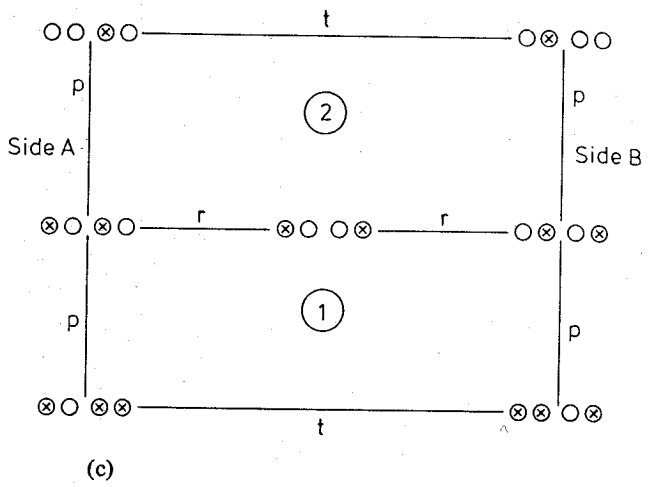

Fig. 4. (a) Graph representing the possible transitions between all 16 proton configurations for a conductor with two groups. (b) Graph representing the possible transitions between the 10 proton configurations with at most (except 0000) either one L_t, D_t, D_r or L_tL_r fault. This graph provides a proper description of the steady-state flux of all pH values as well as for small electric fields ($\Delta U < 0.1$ V). The letters r, t and p denote the type of transition, i.e. rotation, translation and protonation or deprotonation of the conductor end groups, respectively. (c) Graph as in (b) representing the possible transitions between 7 proton configurations. Cycles 1 and 2 provide a proper description of the steady-state flux for $pH_B < 7$ and $pH_A < 9$.

which entails three faults $L_tL_rL_t$ opens a new conduction pathway important at large pH. Inclusion of this configuration in a calculation according to the graph in fig. 4b yields the same flux as the full calculation over the entire pH range. This indicates that the most probable configurations for the conductor are those deviating by only two or three faults from either of the two "no fault" equilibrium configurations. In reality the energy of the proton configuration 0000 is too large (due to the L_t–L_t fault interaction) to play a significant role. However with increasing length of the conductor ($N > 4$) this configuration is replaced by configurations with one L_r and two L_t faults, the L_t faults being separated by one or more conductor groups such that the L_t–L_t interaction is small. When both solutions become basic [pH > pK(XH)], configurations entailing a negative ionic fault L_t at both conductor ends contribute to the proton transport. For longer conductors there exist many such states, but since they contribute only at high pH, calculations performed on larger sys-

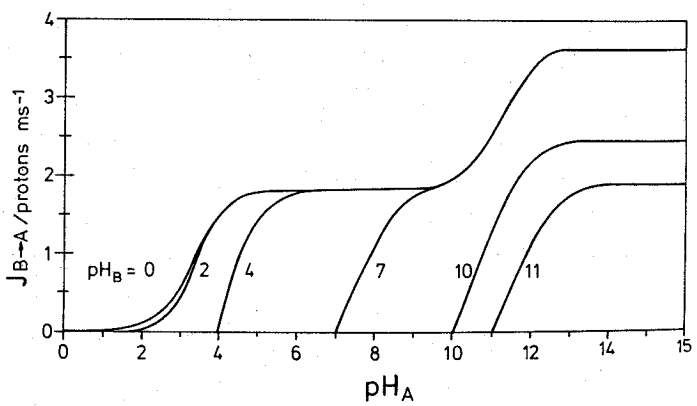

Fig. 5. Steady-state proton flux $J_{B\to A}$ through a conductor with two groups (N = 2) as a function of pH_A, at pH_B = 0, 2, 4, 7, 9, 11. The calculations employed all the 16 possible proton configurations in fig. 4a.

tems with $pH_B < 7$ may include only configurations with a maximum of two faults.

To rationalize the flux curves in fig. 3, it is illuminating to consider in detail the proton configurations involved in the conduction process. The transport of protons from B to A is achieved by closed cycles in the configuration graph. There are five such cycles which contribute to the $N = 2$ chain transport and can be followed in fig. 4b. In the binary number representation they are:

cycle 1: 0101 → 1001 → 1010 → 1011 → 1101 → 0101,
cycle 2: 0101 → 1001 → 1010 → 0010 → 0100 → 0101,
cycle 3: 0101 → 1001 → 0001 → 0010 → 0100 → 0101,
cycle 4: 0001 → 0010 → 0100 → 1000 → 1001 → 0001,
cycle 5: 0001 → 0010 → 0100 → 1000 → 0000 → 0001. (8.1)

The proton concentrations in solutions A and B, i.e. pH_A and pH_B, determine the contribution of each cycle to the transport. Obviously, cycle 1 is important when both solutions are acidic, whereas cycles 2 to 5 are important when the solutions are basic.

The proton flux from solution B to solution A over a large pH range as predicted by a calculation accounting for all 16 proton configurations of a $N = 2$ chain is presented in fig. 5. As long as B is acidic, the proton flux increases in two steps resembling a titration curve. The first step occurs when cycle 1 in (8.1) is completed as the deprotonation at A 1101 → 0101 becomes possible at $pH_A = pK(XH_2^+) = 3$. Cycle 1 and 2 both pass through the L_r fault 1001 which has an activation energy of 0.44 eV (see table 2 and fig. 2) and a formation rate

$$J_{max} = K_{0101 \to 1001} = 3.61 \text{ proton ms}^{-1}. \quad (8.2)$$

Since the activation energies of all the other transitions are smaller, the transition sequence 0101 → 1001 → 1010 is rate limiting for the proton flux through cycles 1 and 2. However, as the configuration 1001 decays with equal probability to 1010 and 0101, the maximum proton flux is only $J_{max}/2$. This value is reached at the first plateau of the flux curves in fig. 5.

The second step of the flux curves occurs when cycle 3 is completed as the proton configuration 1001 starts to decay through 0001 at $pH_A = pK(XH) = 10$ rather than through 1010 as in cycle 1 and 2. In cycle 3 the formation of the L_r fault 1001 is still rate limiting. At high pH_A, however, the decay of this configuration is preferentially to 0001 and, as a result, the proton flux assumes the full value J_{max} as shown in fig. 5.

When solution B is basic, the first plateau of the flux curve disappears and the height of the second plateau diminishes since now a portion of the flux goes through cycles 4 and 5 which are not as efficient as cycle 3. The maximum possible flux through cycles 4 and 5 is also determined by the rate of a $0 \to L_r$ transition, i.e. 0100 → 1000. However, both cycles entail the transition sequence 0001 → 0010 → 0100 → 1000 with the configurations 0010 and 0100 connected by a very fast proton translation. There is then equal opportunity at these configurations that the cycle ends up at the forward configuration 1000 or at the backward configuration 0001. Therefore, the maximum possible flux is reduced to $J_{max}/2$. This reduction of the flux is observed in fig. 5 for $pH_B = 11$ in which case the protons flow predominantly through cycles 4 and 5. At still larger values of pH_B, the proton flux will cease totally as the protonation rate K_P becomes too small.

Calculations for conductors with more than two elements ($N > 2$) have been performed accounting only for $(N+1)^2$ proton configurations. The configurations were selected by limiting their energy of formation by $E_F^{max} = 0.38$ eV. With this criterion all configurations which contain any double faults, except L_tL_r faults, were neglected. Calculations for $N = 2, 3$ have shown us that with this limitation, the steady-state proton flux is accurately described for $pH_B < 7$, at all possible pH_A values, and for small electric potential gradients $|U_B - U_A| \leqslant 0.1$ eV. For $pH_B > 7$ the proton flux does not depend on the length of the conductor, i.e. for this pH_B range the $N = 2$ calculations above entail the desired information.

Fig. 6 presents the proton flux across conductors of various lengths as a function of $pH_A - pH_B$, for $pH_B = 0$ and $pH_B = 7$. The flux curves exhibit qualitatively the same features as discussed earlier for $N = 2$. However, the height of the first plateau, $J_1(N)$ decreases with N according to

$$J_1(N) = J_{max}/N. \quad (8.3)$$

To understand this behaviour one needs only to consider the configuration graph in fig. 7 which in the pH-region of the first step suffices to describe the proton conduction. Since translations are much faster than rotations, the latter are normally rate determining. The

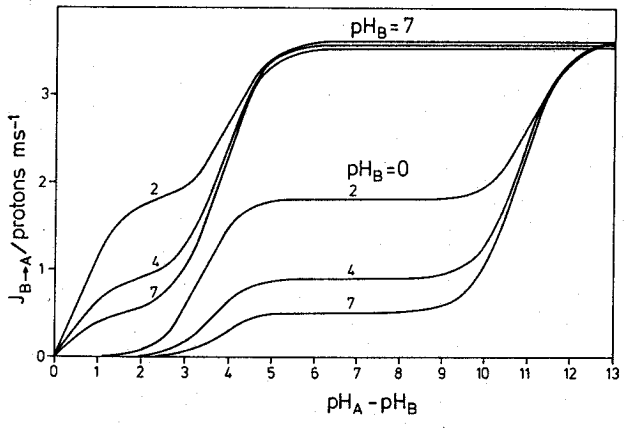

Fig. 6. Steady-state proton flux $J_{B\to A}$ through conductors of length $N = 2, 4, 7$ as a function of $pH_A - pH_B$ at $pH_B = 0$ and $pH_B = 7$. The calculations accounted for only a reduced number of proton configurations satisfying $E_F^{max} = 0.38$ eV (see text).

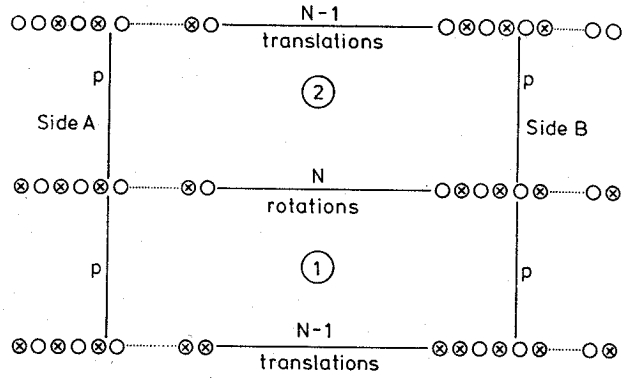

Fig. 7. Graph of proton configurations employed in the calculation of fig. 6 for $pH_B < 7$ and $pH_A < 9$. The graph contains $3N + 1$ configurations and is a generalization of fig. 4c to arbitrary N.

probability for an initial rotation creating a L_r fault at a conductor end is very small compared to the migration of a L_r fault from one end of the conductor to the other. The dynamics of the motion of a L_r fault can be considered a Gambler's Ruin problem, i.e. a one-dimensional random walk on a discrete grid of $N - 1$ points between two absorbing walls. The probability $P_{A\to B}(N, s)$ that a L_r fault created at end A of the conductor migrates to end B is [26]

$$P_{A\to B}(N, s) = (s - 1)(s^N - 1)^{-1}, \qquad (8.4)$$

where s is the ratio of the probability that the fault L_r rotates toward A to the probability that it rotates toward B. The flux at the first plateau $J_1(N)$ can then be expressed

$$J_1(N) = J_{max} P_{A\to B}(N, s), \qquad (8.5)$$

where J_{max} has to be taken from eq. (8.7). In the limit $s \to 1$ (rotations to the left or right are equally probable), we obtain eq. (8.3). Under acidic conditions, the longer the conductor the less efficiently it transports protons across the membrane. When at least one or both sides of the membrane are basic, $pH > pK(XH)$, the length is no longer important since a L_r fault once created at the A end moves directly to the B end.

We like to consider now the influence of an applied electric potential on the flux of protons. In fig. 8 the proton flux for conductors of varying length is presented as a function of the electric potential difference $|U_B - U_A|$ for $pH_A = pH_B = 7$. The curves exhibit a linear dependence of the flux on $U_B - U_A$, i.e. they reflect Ohm's law for proton conduction: $J_{BA} = R(N)^{-1}(U_B - U_A)$. One can then attribute a resistance $R(N)$ to the whole chain and a resistance R_E to its individual elements. The corresponding resistance values $R(N)$ are given below fig. 8. The values fit the expression

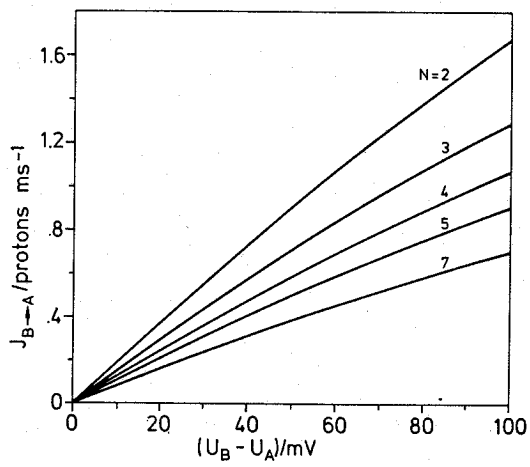

Fig. 8. Electric potential dependence of the steady-state proton flux $J_{B\to A}$ through conductors of length $N = 2, 3, 4, 5, 7$ at $pH_A = pH_B = 7$. The calculations accounted for all proton configurations which entail at most either one L_t, D_t, L_r, or L_tL_r fault. The linear approximation $J_{B\to A} = R^{-1}(N)(U_B - U_A)$ yields for $U_B - U_A < 30$ mV the resistance values (in mV ms protons^{-1}) 54.7, 69.3, 83.9, 98.4 and 127.5 for $N = 2, 3, 4, 5$ and 7, respectively.

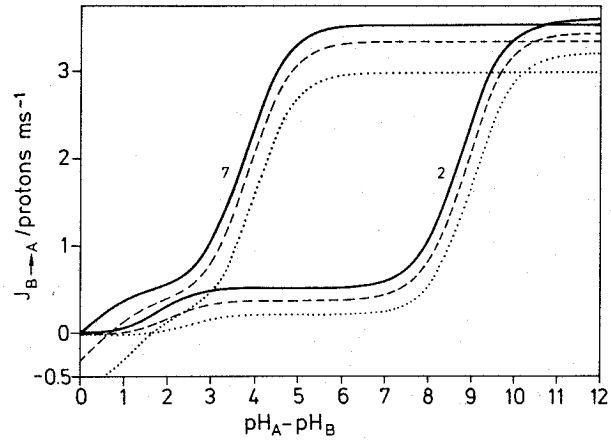

Fig. 9. Steady-state proton flux $J_{B\to A}$ through a conductor with 7 groups as a function of $pH_A - pH_B$ at $pH_B = 2$ and $pH_B = 7$ with a retarding electrical potential $U_B - U_A = 0$, -40, -100 mV. The calculations accounted only for proton configurations entailing at most either one L_t, D_t, L_r, or L_tL_r fault.

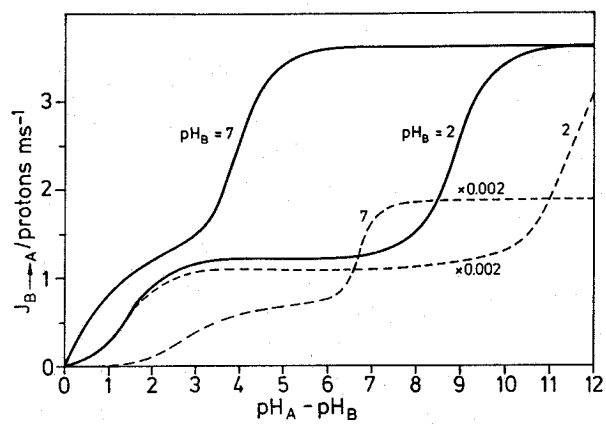

Fig. 10. Steady-state proton flux $J_{B\to A}$ through a conductor of length $N = 3$ for rotational frequency factors $A = 10^{11}$ s^{-1} (——, case I) and $A = 5 \times 10^{13}$ s^{-1} (– – –, case II). The calculation accounted for all proton configurations.

$$R(N) = NR_E + R_0, \tag{8.6}$$

where $R_E = 14.5$ mV ms protons^{-1} and $R_0 = 26.0$ mV ms protons^{-1}. R_0 accounts for a contact resistance between the solvent and the membrane conductor independent of the length of the conductor. R_0 is pH dependent and has a maximum value at pH = 7.

Fig. 9 shows the proton flux evaluated for a conductor with $N = 7$ elements as a function of pH under the influence of a retarding electric potential U. The potential gradient causes an overall reduction, but does not change the qualitative behaviour of the proton flux. Since the maximum flow of protons is determined by the rate of formation of an L_r fault, we can use eqs. (5.4) and (5.5) to calculate the reduction upon applying an electric gradient across the membrane*

$$\overleftarrow{k}^{\text{elect}}(0 \to L_r) = k(0 \to L_r) \exp[-\beta\mu_r(U_B - U_A)/2d]. \tag{8.7}$$

According to eqs. (5.4) and (5.5) μ_r/d assumes the value 0.056 for $N = 7$ and the rates are

$$\overleftarrow{k}^{\text{elect}}(0 \to L_r) = 3230 \text{ protons s}^{-1}$$

$$\text{for } |U_B - U_A| = 0.1 \text{ V},$$

$$= 3450 \text{ protons s}^{-1} \tag{8.8}$$

$$\text{for } |U_B - U_A| = 0.04 \text{ V},$$

in good agreement with the numerical values of J_{max} in fig. 9.

The proton flux corresponding to the first plateau can be determined from eqs. (8.4) and (8.5) with

$$s = \exp[-\beta\mu_r|U_B - U_A|/d]$$

and J_{max} taken from eq. (8.8). For the potential gradients 0.1 V and 0.04 V, the flux $J_{B\to A}$ is 217 and 373 protons s^{-1}, respectively.

Finally we like to discuss the possibility that the rate constants for rotation and translation processes are of comparable magnitude. For this purpose, we assume a 500-fold increase of the frequency factor A_{ij} for L_r and D_r fault migration. Fig. 10 presents the proton flux for a conductor with $N = 3$ predicted for case I of the old frequency factors and that predicted for case II of the new frequency factors. In our calculation we have included all possible proton configurations. For a comparison of case I and II to be meaningful the fluxes II have been rescaled by the factor 0.002. This factor represents the ratio of the rate constants for L_r fault formation

$$J_{max} = K_{010101\to 100101},$$

which is rate limiting for the overall conduction process (see above).

Fig. 10 demonstrates that the "titration" behaviour of the flux curves, indicating transitions between conduction cycles, as discussed above, does not change qualitatively in going from case I to case II. However,

the titration steps are shifted to higher pH_A values and the flux values are suppressed relative to J_{max}. The pH shift is due to the fact that the conduction process has to pass through the deprotonation step *at side A* described by

$$K_D = K_{101001 \rightarrow 101000} \approx 2 \times 10^7, \quad pH_A = 11,$$

$$\approx 2 \times 10^9, \quad pH_A = 13$$

and is counteracted by the rotation process described by

$$k_r = K_{101001 \rightarrow 101010} \approx 10^7 \text{ s}^{-1}, \quad \text{case I},$$

$$\approx 4 \times 10^9 \text{ s}^{-1}, \text{ case II}.$$

In case I $K_D > k_r$ already at $pH_A = 11$, and, hence, the flux approaches its maximum value for $pH_A \geq 11$. In case II, however, $K_D \ll k_r$ at $pH_A = 11$ and only at $pH_A = 13$ one has $K_D \approx k_r$, i.e. larger pH_A values are needed to bring about the maximum proton flow.

The general suppression of the proton flux relative to J_{max} is readily explained by noting that the formation of the L_r fault $101010 \rightarrow 101001$ is so fast in case II ($k_r' = J_{max} = 2 \times 10^6 \text{ s}^{-1}$) that it is no longer absolutely rate limiting for the overall conduction cycle at medium pH values

$$101010 \xrightarrow{k_r'} 101001 \xrightarrow{k_r} 100101 \xrightarrow{k_r} 010101 \xrightarrow{K_P} 110101$$

$$\xrightarrow{k_t} 101101 \xrightarrow{k_t} 101011 \xrightarrow{K_D} 101010.$$

In fact, one has $K_D = 2 \times 10^7 \text{ s}^{-1}$ for $pH_A \leq 11$, i.e. one expects at $pH_B = 2$ a slight decrease of the proton current below the $J_{max}/3$ value. At $pH_B = 7$ one has $K_P = 2 \times 10^{10-pH_B} \text{ s}^{-1} = 2 \times 10^3 \text{ s}^{-1}$, a rate constant which is much smaller than k_r' and, hence, K_P will determine the proton current.

9. Conclusion

To determine the steady-state proton flux across a membrane along the one-dimensional conductor schematically drawn in fig. 1, not all degrees of protonation need be considered. Only those configurations in which the conductor deviates slightly from either of the equilibrium configurations are required to describe the various pH dependent transport mechanisms. Using the data from kinetic studies of the proton transport in ice, we determined that the maximum flux possible from such a conductor is limited by the rate of injecting an L-Bjerrum like defect into the system. The value $J_{max} = 3.61$ protons ms^{-1} compares well with the proton pump rate in halobacterium halobium [2], and while its pump cycle is a problem of dynamic and not passive transport, the appearance of an L-Bjerrum defect, i.e. group rotation, is necessary to bring the system back to its original state. If the protons are really transported along a hydrogen-bonded network, the study of the passive transfer of protons across the membrane will also be useful in determining what mechanisms will be important in the dynamic transport. For example, the configurations in cycle 1 of fig. 4b are just those employed by Nagle and Morowitz [9] to study the dynamic relaxation of the hydrogen-bonded conductor once an excess proton (D_t fault) is injected by the ATP mechanism at one end. If the solutions A and B become very basic, cycle 2 of fig. 4c along with the cycles corresponding to those numbered 3, 4 and 5 in fig. 4b would be necessary to treat the dynamics.

Perhaps the most serious criticism of such models for the proton transport is the special physical requirement of a protein assuming the proper geometry and its specialization to the transport of only protons and no other positive ions. The X-ray structure work of Dunker and Marvin [6] has shown that the required protein alignment occurs in many membranes, and that by slight distortions their amino acid side groups could be aligned to form a hydrogen-bonded pathway. The recently obtained complete sequence of the protein bacteriorhodopsin of halobacterium halobium and first attempts to deduce its tertiary structure encourage the notion of a proton channel formed by a continuous chain of hydrogen bonds as considered in this paper [27].

Finally, we would like to emphasize that it is by no means clear that the rate constants describing proton conduction in proteins resemble those of ice-like systems. Group rotations may be considerably faster in proteins than in ice, whereas proton translation could be rather slow as biological proton conductors should prefer groups with pK values near the physiological pH values in order to reduce the free energy requirement of injecting L-Bjerrum like defects, i.e. injecting or withdrawing protons. The agreement of proton conduction rates of ice-like systems and that of bacterio-

rhodopsin, if the latter involves at all a hydrogen bridge network, may be fortuitous. One may rather expect that proton conduction through proteins exhibits rather different, possibly much faster, rates and is rate-limited by other proton configurations and conduction cycles than those discussed above. In this respect we have outlined, however, a suitable theoretical framework for appropriate future descriptions.

Acknowledgement

The authors would like to thank J.F. Nagle and H.J. Morowitz for sending preprints of their work. We are grateful to Professor Manfred Eigen for helpful comments and to Professor Albert Weller for his continuous support. The use of the computing facilities of the Gesellschaft für wissenschaftliche Datenverarbeitung mbH is gratefully acknowledged.

References

[1] P. Mitchell, Nature 191 (1961) 144.
[2] R. Henderson, A. Rev. Biophys. Bioengng. 6 (1977) 87.
[3] H.T. Witt, in: Bioenergetics of photosynthesis, ed. Govindjee (Academic Press, New York, 1975) pp. 493–554;
A.T. Jagendorf, in: Bioenergetics of photosynthesis, ed. Govindjee (Academic Press, New York, 1975) pp. 413–492.
[4] L. Onsager, in: The neurosciences, ed. F.O. Schmitt (Rockefeller University Press, 1967) pp. 75–79; in: Nobel lecture: chemistry, The Motion of Ions, Principles and Concepts (Nobel Foundation, Stockholm, 1968).
[5] A.K. Dunker, J. Supramolec. Struct. S1 (1977) 659.
[6] A.K. Dunker and R.K. Marvin, J. Theoret. Biol. 72 (1978) 9.
[7] J.F. Nagle and H.J. Morowitz, Proc. Natl. Acad. Sci. USA 75 (1978) 298.
[8] H.J. Morowitz, in: Advan. Biol. Med. Phys., to be published.
[9] J.F. Nagle and H.J. Morowitz, preprints.
[10] L. Glässer, Chem. Rev. 75 (1975) 21. A major review article on hydrogen-bonded systems in chemistry and biology.
[11] S.F. Fischer, G.L. Hofacker and J.R. Sabin, Phys. Kondens. Materie 8 (1969) 268;
J.K. Fung, K. Godzik, G.L. Hofacker, Ber. Bunsenges. Physik. Chem. 77 (1973) 980.
[12] A. Kuwada, A.R. McGhie and M.M. Labes, J. Chem. Phys. 52 (1970) 3121.
[13] V. Schmidt, J. Drumheller and F. Howell, Phys. Rev. B4 (1971) 4582.
[14] P.V. Hobbs, Ice physics (Clarendon Press, Oxford, 1974).
[15] N. Bjerrum, Science 115 (1952) 385.
[16] Mou-Shen Chen, L. Onsager, J. Bonner and J. Nagle, J. Chem. Phys. 60 (1974) 405.
[17] N.H. Fletcher, The chemical physics of ice (Cambridge University Press, Cambridge, 1970).
[18] L. Onsager, in: Physics and chemistry of ice, ed. E. Whalley (Royal Society of Canada, Ottawa, 1973) pp. 7–12.
[19] M. Eigen and L. DeMaeyer, in: The structure of electrolytic solutions, ed. W.J. Hamer (Wiley and Sons, New York, 1959) pp. 64–85.
[20] C. Jaccard, Ann. N.Y. Acad. Sci. 125 (1965) 390.
[21] J.H. Bligram and H. Granicher, Phys. Cond. Matter 18 (1974) 275.
[22] M. Eigen and L. DeMaeyer, Proc. Roy. Soc. London A247 (1958) 505.
[23] A.L. Lehninger, Biochemistry (Worth Publishers, New York, 1972) ch. 4.
[24] M. Eigen, Z. Phys. Chem. NF1 (1954) 176;
G.G. Hames, Principles of chemical kinetics (Academic Press, New York, 1978) chs. 2 and 8.
[25] L. Onsager and M. Dupuis, in: Electrolytes, ed. B. Pesce (Pergamon Press, Oxford, 1962) p. 27.
[26] W. Feller, An introduction to probability theory and its application, Vol. 1 (Wiley, New York, 1968) pp. 344–345.
[27] Yu.A. Orchinuikov, N.G. Abdulaev, M.Yu. Feigina, A.V. Kiselev and N.A. Lobanov, FEBS Letters 100 (1979) 219.